Available online at www.sciencedirect.com

ScienceDirect

Scripta Materialia 60 (2009) 803–806

Scripta MATERIALIA

www.elsevier.com/locate/scriptamat

Evaluation of thermal fatigue damage of 200-nm-thick Au interconnect lines

M. Wang,[a,b] B. Zhang,[b] G.P. Zhang[a,*] and C.S. Liu[b]

[a]*Shenyang National Laboratory for Materials Science, Institute of Metal Research, Chinese Academy of Sciences, 72 Wenhua Road, Shenyang 110016, People's Republic of China*

[b]*School of Materials & Metallurgy, Northeastern University, 3-11 Wenhua Road, Shenyang 110004, People's Republic of China*

Received 6 January 2009; accepted 18 January 2009
Available online 3 February 2009

Thermal fatigue properties of 200-nm-thick Au interconnects with a width of 2 μm were evaluated by applying alternating current. We found that the temperature distribution along the Au interconnect can be described by a simplified one-dimensional equation of heat conduction. The lifetime as a function of thermal cyclic strain range ($\Delta\varepsilon$) for the narrow Au lines follows the conventional Coffin–Manson relationship when $\Delta\varepsilon \leqslant 0.47\%$, while the number of cycles to failure extends to an engineering-defined high-cycle fatigue region.

Keywords: Au film; Thermal fatigue; Alternating current

Metallization interconnects in microelectronic circuits experience extreme conditions during fabrication and service, including relatively high temperature, high current density and thermal cyclic strain. Consequently, three typical kinds of failure modes can affect the reliability of the interconnect: electromigration (EM), stress-induced voiding (SIV) and thermal fatigue. Both EM and SIV had been actively investigated for several decades [1]. Thermal fatigue comes from the time-varying temperature in the interconnect during its service due to the power dissipation within the interconnect and the surrounding structures. The variation in temperature creates time-varying thermal strain due to the thermal expansion mismatch between the metal line and the surrounding material, which can lead to the formation of thermal cyclic strain-induced damage. Even though several observations of fatigue in thin metal films at room temperature have shown that fatigue properties, damage behavior and dislocation structures of the metal films are quite different from that of their bulk counterparts when the film thickness is on the sub-micrometer scale [2–10], limited work on thermal cyclic strain-induced damage behavior has been conducted for the narrower metal lines [11–16], which is becoming a more and more important reliability issue. In this paper, thermal fatigue damage of a 200-nm-thick Au interconnect generated by alternating current (AC) are investigated. The temperature distribution along the Au lines under AC-induced cyclic Joule heating was analyzed theoretically, and failure lifetimes of the Au lines were evaluated.

A 200-nm-thick Au film were deposited onto a quartz substrate by a radiofrequency magnetron sputtering system under a high vacuum. X-ray diffraction θ–2θ scans show that the grains in the Au film have a (1 1 1) out-of plane texture, as shown in Figure 1(a). The grain size of the Au film was estimated as 74.0 ± 11.1 nm by scanning electron microscopy (SEM; LEO Supra 35), as shown in the inset of Figure 1(a). Subsequently, a set of the Au interconnect lines 2 μm in width and 50 μm in length were fabricated by a focused-ion-beam (FEI Nova200 NanoLab) milling technique under a beam current of 50 pA. In order to have a smooth side surface of the metal line, a fine beam current of 10 pA at a low accelerating voltage of 5 keV was finally used to clean all the sides of the metal line.

In terms of the basic idea proposed by Mönig et al. [14], the Au lines were tested in situ by applying AC. The principle for such a testing system is based on the fact that AC-induced Joule heating of a metal film bonded to a substrate potentially causes thermal cyclic strain due to the difference in thermal expansion coeffi-

* Corresponding author. Tel./fax: +86 24 23971938; e-mail: gpzhang@imr.ac.cn

1359-6462/$ - see front matter
doi:10.1016/j.scriptamat.2009.01.024

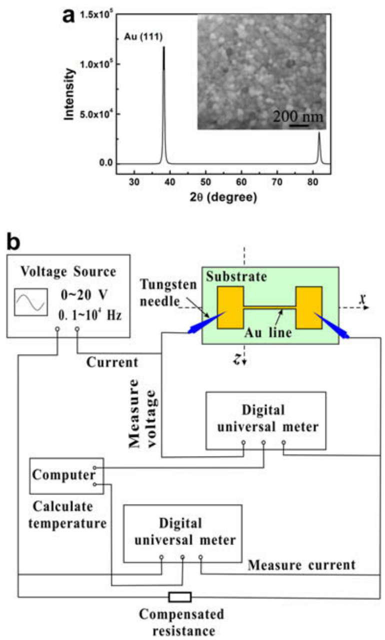

Figure 1. (a) X-ray diffraction of 200-nm-thick Au film. (b) Schematic diagram of a testing set-up for thin metal interconnect line subjected to AC.

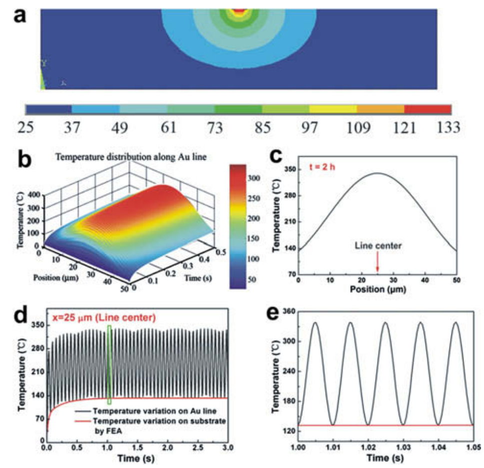

Figure 2. Temperature distribution (a) in the silica substrate beneath the Au interconnect line, which is subjected to AC with the rms current density of 5.3 MA cm^{-2} (based on finite element analysis) and (b) along the Au line as a function of position and time (based on Eq. (4)). (c) Cross-sectional view of (b) in a certain cyclic time of $t = 2$ h; (d) the cross-sectional view of (b) in a certain position of $x = 25$ μm; (e) partially enlarged drawing of the squared region in (d).

cients between the metal line and the underlying substrate. Figure 1(b) schematically depicts the testing system we used. Here, the AC with a sinusoidal wave and a frequency of 50 Hz was applied to the Au line through two tungsten needles controlled by two micromanipulators, as schematically illustrated in Figure 1(b). By comparing the experimental resistance of the Au line with the theoretical resistance calculated by $R = \rho \times \frac{l}{s}$, we found that the difference between them was very small. The effect of the contact resistance between the tungsten needles and the Au pads could therefore be neglected. The root mean square (rms) current density (I_{rms}) of the applied AC varied from 3.5 to 11.5 MA cm^{-2}, which was expected to generate a temperature cycle with a range ΔT in the Au lines. The total strain range applied to the Au line can be estimated by $\Delta\varepsilon = (\alpha_{Cu} - \alpha_{SiO_2}) \cdot \Delta T$ based on coefficients of thermal expansion (CTE) of gold ($\alpha_{Au} = 1.42 \times 10^{-5}$ K^{-1}) and silicon dioxide ($\alpha_{SiO_2} = 5.5 \times 10^{-7}$ K^{-1}). The lifetime, i.e., the total number of cycles to failure, was recorded at the moment when the Au line is broken.

It is necessary to determine the AC-generated temperature distribution along the Au line prior to examining damage behavior. The temperature distribution of the substrate beneath the Au interconnect under $I_{rms} = 5.3$ MA cm^{-2} was calculated first by finite element analysis (FEA). The substrate temperature beneath the Au interconnect was described by the red region in Figure 2(a). It is clear that the temperature of the substrate can reach the steady magnitude of 133 °C in a very short time. Thus, the substrate temperature can be regarded as a heat reservoir and directly corresponds to the lowest temperature of the Au line. Mönig et al. [14] reported that the temperature of the Si substrate beneath the Cu interconnect was about 100 °C, as evaluated by FEA. This is due to the fact that the coefficient of thermal conductivity of silicon dioxide is far lower than that of Si. It is assumed that the AC-generated Joule heating in the Au line would disperse mainly towards the two pads, but rather less in air due to the pad areas being much larger than that of the Au line and the lower convection coefficient of the air. According to Fourier's law, the heat flow rate per unit area can be expressed as

$$q = -k \times \nabla T = -k \times \frac{\partial T}{\partial x} \tag{1}$$

where k is the coefficient of thermal conductivity of the Au line. The differential equation of thermal conduction is established based on the first law of thermodynamics, which can be written as

$$\Delta E = \Delta Q + W \tag{2}$$

where ΔE is the increment of internal energy in the system, ΔQ is the increment of calorific power in the system and W is the work of the system obtained from the external condition. In this case, W is equal to zero. The first law of thermodynamics is applied to the differential system, $dxdydz$, as depicted in Figure 1(b). Eq. (2) then becomes

$$\left[q - \left(q + \frac{\partial q}{\partial x}dx\right)\right] \times dydz + \frac{P(t)}{V} \times dxdydz = \rho c \times \frac{\partial T}{\partial t} \times dxdydz. \tag{3}$$

Eq. (1) can be substituted into Eq. (3) and the differential equation of thermal conduction of the one-dimensional transient temperature field can be obtained as:

$$\rho c \times \frac{\partial T}{\partial t} - k\frac{\partial^2 T}{\partial x^2} = \frac{P(t)}{V} \tag{4}$$

The original and boundary conditions are given as $T(x, 0)$; $T(0, t) = T(50, t) = f(t)$, where $f(t)$ is the functional variation of the substrate temperature. $T_x(25, t) = 0$; $0 < x < 50$ μm and $t > 0$ s. Letting $I_{rms} = 5.3$ MA cm^{-2}, an analytic solution of the temperature (T) as a function of the position from the left side of the Au line (x) and the cyclic time (t) was solved, and the temperature distribution along the Au line is presented in Figure 2(b). Two clear features can be seen in Figure 2(b). First, at a certain cyclic time, the temperature along the Au line exhibits a gradient distribution. The highest temperature appears in the middle of the Au line while the lowest one occurs on both sides of the Au line close to the two pads. Secondly, with increasing cyclic time the temperature of the Au line increases rapidly to a steady state, then slowly in a sinusoidal variation. A cross-sectional view of the temperature distribution along the Au line after cyclic Joule heating for 2 h is shown in Figure 2(c). It is clear that the temperature in the middle of the Au line is close to 343 °C and gradually decreases down to about 133 °C at both sides of the Au line close to the two pads. Figure 2(d) shows that the temperature of the Au line reaches 133 °C rapidly (within about 1 s) and then varies in a sinusoidal wave with a range of $\Delta T = 210$ °C with cyclic time. An enlarged curve of the squared region in Figure 2(d) reveals that the temperature in the middle of the Au line also increases gradually in a sinusoidal variation, and the variable periodic time was half of the AC (see Fig. 2(e)).

It is worth noting that the above analysis of the temperature distribution along the Au line depends on the line dimensions, such as the size of the pad and the length of the line, which control the dissipation of the Joule heat in the line. The fact that the length of the Au line used here is shorter than that used by Mönig et al. [14] and Keller et al. [17] means that the ability to store the heat in the Au line is significantly decreased. As a result, there was an evident gradient distribution of temperature in the Au line, which led to more severe damage in the middle of the Au line than at other places along the line. The above theoretical calculation of the temperature distribution along the Au line can be demonstrated by the following SEM observations of the damage morphology at the line surface.

From Figure 2(b), the difference in temperature between the Au line and the substrate in the steady state was obtained as $\Delta T = 210$ °C in the case of $I_{rms} = 5.3$ MA cm^{-2}. Thus, the thermal cyclic strain range can be calculated as $\Delta\varepsilon = 0.27\%$, which was applied to the as-deposited Au line shown in Figure 3(a). Figure 3(b)–(f) presents damage morphologies of the Au line after 7.45×10^6 cycles under $\Delta\varepsilon = 0.27\%$ generated by AC. Figure 3(b) reveals that the Au line was broken in the middle due to the local melting. The damage became more extensive and severe the closer the position to the middle of the Au line. In particular, the top and side surfaces of the Au line close to the middle part became much rougher. Closer inspection shows that the grains close to the pad did not grow (see Fig. 3(c)), while those close to the middle part of the line have grown much larger and have even become somewhat faceted, as shown in Figure 3(d). This indirectly demonstrates that temperature is distributed inhomogeneously along the Au lines. The grain growth in the thin film can be described as [18],

$$r^2 - r_0^2 = \alpha_0 \exp\left(-\frac{Q}{kT}\right)t, \tag{5}$$

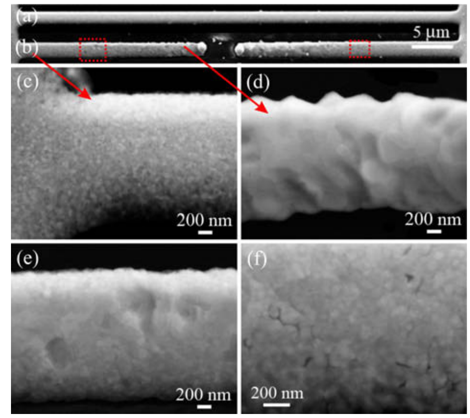

Figure 3. SEM images of the Au line after 7.45×10^6 cycles under $\Delta\varepsilon = 0.27\%$. (a and b) Whole views of the Au line before and after experiment, respectively; (c and d) high magnification of the arrowed regions in (b); (e and f) close observations of the squared regions in (b).

where r is the average grain radius after a time t, r_0 is the average initial grain radius, α_0 is a weakly temperature-dependent constant, Q is the activation energy for grain boundary motion and k is the Boltzmann constant. Using Eq. (5) and the values based on the SEM observations, the temperature in the middle of the Au line was estimated as $T \approx 400$ °C after 7.45×10^6 cycles. Compared with the result from the grain growth model, it was found that the temperature calculated by the equation of thermal conduction (Eq. (4)) is less than 57 °C. This demonstrates that it is reasonable to describe the temperature variation with the differential equation of thermal conduction of a one-dimensional transient temperature field.

The thermal fatigue damage morphologies shown in Figure 3(e) and (f) are different from the results reported by Park et al. [16]. Several wedge-shaped pits formed in the Au line, as indicated by the arrows in Figure 3(e). The size of the center of the pits approximates to a grain size, while the external size of the pits is 500 ± 50 nm. The other damage behavior identified was the formation of microcracks at triple junctions (see Fig. 3(f)). Owing to the small grain size (several tens of nanometers) of the present Au line, the wrinkles found in the Cu line with micron-scale grains by Mönig et al. [13] were not observed here. In contrast, the different damage behaviors at the different locations of the Au line (see Fig. 3(b)–(f)) are attributed to the effect of different amplitudes of thermal cyclic strain or the temperature.

Figure 4 presents the relation between the thermal strain range ($\Delta\varepsilon$) generated by AC and the number of cycles to failure (N_f) of the Au lines. The thermal fatigue lifetime significantly decreases with increasing $\Delta\varepsilon$. Specifically, Figure 4 can be divided into two regions, corresponding to the low strain range (region I) and the high strain range (region II). In region I ($\Delta\varepsilon \leqslant 0.47\%$), $N_f \sim \Delta\varepsilon$ follows the conventional Coffin–Manson relationship, with a fatigue strength exponent of −0.5. This value is close to that of most bulk metals [19]. This indicates that under $\Delta\varepsilon \leqslant 0.47\%$ (corresponding to $I_{rms} < 8$ MA cm^{-2}) the damage behavior of the thin Au line with a line width of 2 μm is controlled by the

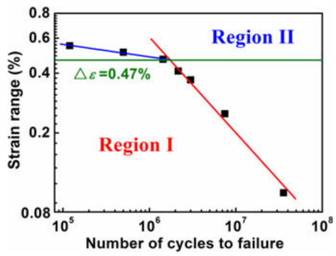

Figure 4. Relationship between the numbers of cycles to failure and the applied strain range generated by AC.

thermal fatigue mechanism even though the number of cycles is above 10^6, which usually belongs to a high-cycle fatigue region. As $\Delta\varepsilon > 0.47\%$, corresponding to region II, the experimental data deviate far from the Coffin–Manson equation. This may be attributed to the excessive effect of the higher current density, which directly led to large Joule heating, causing the Au lines to rapidly melt and fail.

Recently, Zhang et al. [20] found that there were low and high cycle regions in thermally fatigued 60-nm-thick Cu lines on an Si substrate with a line width ranging from 5 to 15 μm. The corresponding thermal strain range varied from about 0.015% to 0.2%. These strain ranges are lower than that of the present study. It should be noted that the CTE of silicon is far larger than that of SiO_2. Thus, compared with the present Au line on a silica substrate, there exists a relatively low strain range in Cu lines on an Si substrate even with the same temperature variation. Specifically, the temperature difference between the metal lines and the substrate applied by Zhang et al. on the Cu lines was not large [20].

In the present study, it is found that under the "low" strain range ($\Delta\varepsilon \leqslant 0.47\%$) the relationship between the cyclic lifetime and the thermal strain range follows a typical Coffin–Manson equation, which can describe well the fatigue lifetime in a low-cycle fatigue region for bulk metals [21]. Generally, when the number of cycles to failure of the bulk metals is more than 10^4–10^5, it is conventionally considered to be high-cycle fatigue. However, the operating lifetime of the metal interconnects in many microelectronic devices is far higher than engineering-defined 10^7 cycles in the practical applications, and can even exceed 10^{12} cycles [22]. Compared with such high cycles, the number of cycles in region I ($\Delta\varepsilon \leqslant 0.47\%$) should belong to the low-cycle fatigue region for thin metal lines even if the fatigue lifetime is much higher than 10^4 cycles. Thus it is not difficult to understand why the $N_f \sim \Delta\varepsilon$ follows the conventional Coffin–Manson relationship in conventional high-cycle fatigue regions.

From our results, it is expected that the so-called high-cycle fatigue behavior of metal lines may extend to ultrahigh cycles at a relatively low strain range. In fact, Park et al. [16] found that the relationship between the cyclic lifetime and the thermal strain range of 200 nm Cu lines could not satisfy the Coffin–Manson equation in the ultrahigh cycle region up to 10^{10} cycles. This further demonstrates that when the size of metal films decreases to the sub-micron scale or less, the fatigue lifetime and behavior is quite different from that of bulk metals, even though the whole relationship between the cyclic lifetime and the strain range is similar to that of bulk metals [7,10,13,16].

In summary, we demonstrated that the temperature distribution along Au interconnect lines generated by AC can be described by a simplified one-dimensional equation of heat conduction. Under a relatively low strain range ($\Delta\varepsilon \leqslant 0.47\%$), the variation with thermal strain in the lifetime of an Au line with a width of 2 μm follows the conventional Coffin–Manson relationship. The damage of thin Au lines is controlled by an AC-induced thermal fatigue mechanism. In contrast, under a high strain range ($\Delta\varepsilon > 0.47\%$), the damage behavior of the Au lines was dominated by excessive Joule heating.

This work was supported by the National Basic Research Program of China (Grant No. 2004CB619303) and by the National Natural Science Foundation of China (Grant Nos. 50471081 and 50571103).

[1] Ch.S. Hau-Riege, Microelectron. Reliab. 44 (2004) 195.
[2] S. Hong, R. Weil, Thin Solid Films 283 (1996) 175.
[3] D.T. Read, Int. J. Fatigue 20 (1998) 203.
[4] R. Schwaiger, O. Kraft, Scripta Mater. 41 (1999) 823.
[5] R. Schwaiger, O. Kraft, Acta Mater. 51 (2003) 195.
[6] O. Kraft, R. Schwaiger, P. Wellner, Mater. Sci. Eng. A 919 (2001) 319.
[7] O. Kraft, P. Wellner, M. Hommel, R. Schwaiger, E. Arzt, Z. Metallkd. 93 (2002) 392.
[8] R. Schwaiger, G. Dehm, O. Kraft, Philos. Mag. 83 (2003) 693.
[9] G.P. Zhang, R. Schwaiger, C.A. Volkert, O. Kraft, Philos. Mag. Lett. 83 (2003) 477.
[10] G.P. Zhang, C.A. Volkert, R. Schwaiger, P. Wellner, E. Arzt, O. Kraft, Acta Mater. 54 (2006) 3127.
[11] E. Philofsky, K. Ravi, K. Hall, J. Black, in: Proceedings of the Ninth Annual Proceeding of Reliability Physics, IEEE, 1971, p. 120.
[12] R.R. Keller, R. Mönig, C.A. Volkert, E. Arzt, R. Schwaiger, O. Kraft, in: Proceedings of the Sixth International Workshop on Stress-Induced Phenomena in Metallization, American Institute of Physics, New York, 2002, p. 119.
[13] R. Mönig, PhD Thesis, University of Stuttgart, Germany, 2005. Available from: <http://elib.uni-stuttgart.de/opus/volltexte/2005/2173>.
[14] R. Mönig, R.R. Keller, C.A. Volkert, Rev. Sci. Instrum. 75 (2004) 4997.
[15] Y.B. Park, R. Mönig, C.A. Volkert, Thin Solid Films 515 (2007) 3254.
[16] Y.B. Park, R. Mönig, C.A. Volkert, Thin Solid Films 504 (2006) 321.
[17] R.R. Keller, R.H. Geiss, Y.W. Cheng, D.T. Read, MRS Symposium Proceedings: h Society, Pittsburgh, PA, 2005,, 2005, of Advanced Interconnect, Materials, Technology and Reliability of Advanced Interconnect. Pittsburgh, PA: Materials Research Society, 863 (2005) 295.
[18] C.V. Thompson, Annu. Rev. Mater. Sci. 20 (1990) 246.
[19] S. Suresh, Fatigue of Materials, Cambridge University Press, Cambridge, 1998.
[20] J. Zhang, J.Y. Zhang, G. Liu, Y. Zhao, X.D. Ding, G.P. Zhang, J. Sun, Scripta Mater. 60 (2009) 230.
[21] H.L. Huang, N.J. Ho, Mater. Sci. Eng. A 293 (2000) 7.
[22] M. Ohring, Reliability and Failure of Electronic Materials and Devices, Academic Press, San Diego, CA, 1998.